Spin diffusion in the Mn^{2+} ion system of II-VI diluted magnetic semiconductor heterostructures

A. A. Maksimov,[1,*] D. R. Yakovlev,[2,3] J. Debus,[2] I. I. Tartakovskii,[1] A. Waag,[4] G. Karczewski,[5] T. Wojtowicz,[5] J. Kossut,[5] and M. Bayer[2]

[1]*Institute of Solid State Physics, Russian Academy of Sciences, 142432 Chernogolovka, Russia*

[2]*Experimentelle Physik 2, Technische Universität Dortmund, 44227 Dortmund, Germany*

[3]*A. F. Ioffe Physical-Technical Institute, Russian Academy of Sciences, 194021 St. Petersburg, Russia*

[4]*Institute of Semiconductor Technology, Braunschweig Technical University, 38106 Braunschweig, Germany*

[5]*Institute of Physics, Polish Academy of Sciences, 02668 Warsaw, Poland*

(Received 24 April 2010; revised manuscript received 4 July 2010; published 23 July 2010)

The magnetization dynamics in diluted magnetic semiconductor heterostructures based on (Zn,Mn)Se and (Cd,Mn)Te were studied optically and simulated numerically. In samples with inhomogeneous magnetic ion distribution, these dynamics are contributed by spin-lattice relaxation and spin diffusion in the Mn spin system. A spin-diffusion coefficient of 7×10^{-8} cm^2/s was evaluated for $Zn_{0.99}Mn_{0.01}Se$ from comparison of experiment and theory. Calculations of the exciton giant Zeeman splitting and the magnetization dynamics in ordered alloys and digitally grown parabolic quantum wells show perfect agreement with the experimental data. In both structure types, spin diffusion contributes essentially to the magnetization dynamics.

DOI: 10.1103/PhysRevB.82.035211 PACS number(s): 75.50.Pp, 78.55.Et, 78.67.De, 78.20.Ls

I. INTRODUCTION

Heterostructures based on II-VI diluted magnetic semiconductors (DMSs), like $Cd_{1-x}Mn_xTe$ or $Zn_{1-x}Mn_xSe$, are considered as model systems for spintronic devices.[1,2] Optical spectroscopy techniques have been conveniently used for investigating their properties due to the strong optical transitions in the vicinity of the band gap observable in, e.g., absorption, reflection, and emission. DMS materials are known for giant magneto-optical effects originating from the strong exchange interaction of free carriers with the localized magnetic moments of Mn^{2+} ions.[3,4]

The spin dynamics of free carriers in DMS are controlled by spin and energy transfer in the coupled system of carriers, magnetic ions, and phonon bath (lattice).[5–7] The fast exchange scattering of carriers on magnetic ions (10^{-12}–10^{-11} s) provides efficient transfer into the Mn system but the further transfer from the Mn spin system to the phonon bath is decelerated by the relatively slow spin-lattice relaxation (SLR) rate in materials with low Mn concentrations of a few percent. Control of dynamical properties of the Mn spins, described by the SLR time, is essential because they may show a bottleneck for high-speed applications.

In II-VI DMS, the SLR time of the localized Mn spins, τ_{SLR}, is controlled by concentration-dependent exchange interactions between the Mn^{2+} ions. It varies by several orders of magnitude from millisecond down to nanosecond with increasing Mn concentration x from 0.004 to 0.11, see Fig. 1(c).[6,8] In absence of SLR for isolated Mn ions such a strong dependence is explained by relaxation within Mn clusters.[9] With increasing Mn concentration, the number of clusters grows as does the cluster size. This shortens the characteristic length for spin transfer from a single Mn ion to a cluster and also accelerates the spin-relaxation processes inside a cluster. It was shown that digital growth of ordered DMS alloys enables redistribution of cluster statistics for the same Mn concentration, thus increasing the role of these clusters.[10] Cluster formation results in a considerable enhancement of SLR confirming their leading role in magnetization relaxation dynamics.

There are some experimental evidences that spin diffusion in the Mn spin system plays an important role in the magnetization dynamics of II-VI DMS. First, the strong dependence of SLR time on Mn concentration can be explained by a nonlocal model of SLR in DMS where the spin diffusion from single Mn^{2+} ions to Mn clusters provides fast SLR.[11] Second, a direct experimental proof of the spin-diffusion contribution to the magnetization relaxation in heteromagnetic DMS structures was reported for $Zn_{0.99}Mn_{0.01}Se/Be_{0.93}Mn_{0.07}Te$ structures with different Mn concentrations in the adjacent layers.[12] The slow SLR in the $Zn_{0.99}Mn_{0.01}Se$ layer is bypassed by spin diffusion through

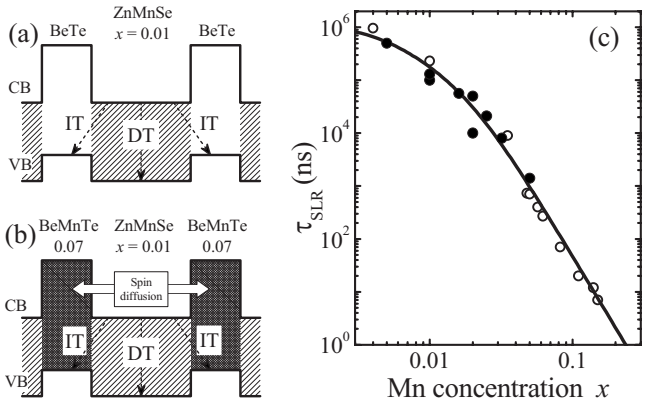

FIG. 1. (a) and (b) Schematic band diagrams of $Zn_{1-x}Mn_xSe/Be_{1-y}Mn_yTe$ quantum wells with type-II band alignment. Dashed arrows show spatially direct (DT) and indirect (IT) optical transitions. Presence of the Mn ions in the $Be_{1-y}Mn_yTe$ layers, see panel (b), opens a new channel for magnetization relaxation in the $Zn_{0.99}Mn_{0.01}Se$ layer via spin diffusion into the $Be_{1-y}Mn_yTe$ layers, see text. (c) Spin-lattice relaxation time as a function of Mn content in II-VI DMS structures based on $Cd_{1-x}Mn_xTe$ (closed circles) and $Zn_{1-x}Mn_xSe$ (open circles) (Ref. 6); the solid line gives the interpolation of these dependences.

the Mn spin system to the $Be_{0.93}Mn_{0.07}Te$ layer with a much faster relaxation rate. Neither experimental nor theoretical reports on a quantitative evaluation of the spin-diffusion parameters in DMS have been published, yet.

The goal of this paper is to provide a detailed experimental study of spin diffusion in the Mn spin system of II-VI DMS and to evaluate the spin-diffusion coefficient. We exploited the potential offered by $Zn_{1-x}Mn_xSe/Be_{1-y}Mn_yTe$ heteromagnetic structures for isolating the spin-diffusion contribution to magnetization relaxation. We also developed a numerical approach to describe the magnetization dynamics in structures with a modulated profile of Mn concentration and approved its validity for $CdTe/Cd_{1-x}Mn_xTe$ digital superlattices and parabolic quantum wells.

II. EXPERIMENTALS

Time-resolved magneto-optical studies of the magnetization dynamics were performed for various $Zn_{1-x}Mn_xSe$- and $Cd_{1-x}Mn_xTe$-based heterostructures grown by molecular-beam epitaxy on (100)-oriented GaAs substrates. Details of the structure designs are given in the sections where the corresponding experimental data are presented. In this paper, we include results for (i) three $Zn_{1-x}Mn_xSe/Be_{1-y}Mn_yTe$ multiple quantum well (MQW) structures with a type-II band alignment, (ii) three $CdTe/Cd_{1-x}Mn_xTe$ digital superlattices, and (iii) two $CdTe/Cd_{1-x}Mn_xTe$ parabolic QWs. The $CdTe/Cd_{1-x}Mn_xTe$ structures were fabricated by the digital growth technique.[13]

We used an all-optical experimental technique to measure the magnetization dynamics,[6,7] exploiting the internal thermometer of the Mn spin temperature T_{Mn}. The giant Zeeman splitting of excitons (band states) is very sensitive to the polarization of the magnetic Mn ions in external magnetic field. The changes in the spectral position of the photoluminescence (PL) line $\Delta E_{PL}(B)$ are proportional to the magnetization changes $\Delta M(B)$, and therefore we obtain by a magneto-optical technique direct information about the magnetization dynamics in DMS. For that purpose, the studied DMS heterostructures were placed in a magnetic field. A pulsed laser was used for heating the Mn spins and the resulting dynamical shift of the PL line with time resolution.

The relaxation of the heated Mn spin system back to bath temperature is described by the magnetization relaxation time τ_{MR} which is contributed by spin-lattice relaxation (with characteristic time τ_{SLR}) and spin diffusion. The relaxation times are equal ($\tau_{MR}=\tau_{SLR}$) for disordered DMS alloys and/or in case, when spatial inhomogeneity in Mn heating does not contribute to the magnetization relaxation. These conditions have been suggested implicitly or explicitly to apply to most of the experiments, but this is not the case for our study, since the structures were designed to promote spin diffusion.

The samples were immersed in pumped liquid helium at $T=1.8$ K, and external magnetic fields B up to 10 T were applied. The magnetic field of a superconducting split-coil solenoid was applied parallel to the structure growth axis (z axis). The photoluminescence signal was detected for right-handed (σ^+) circular polarization, which is the strongest component in magnetic field.

A pump-probe technique with time-resolved detection of the PL excited by the probe-laser pulses was implemented experimentally. A pulsed neodymium-doped yttrium aluminum garnet laser with photon energy of 3.49 eV (wavelength of 355 nm) was used as pump to heat the Mn spin system, emitting pulses with 5 ns duration at a repetition frequency from 100 Hz up to 5 kHz. Excitation power densities up to $\gtrsim 200$ kW/cm^2 could be reached. A semiconductor laser (photon energy 3.06 eV, wavelength 405 nm) with external amplitude modulation served as probe laser, that emitted pulses with duration from 0.5 up to 1 ms synchronized with the pump pulses. The time delay between the pump and probe pulses was varied by a digital delay generator from 0 up to 100 μs. The excitation density of the probe laser was kept below 0.1 W/cm^2 in order to minimize its contribution to heating the Mn spin system. Time-resolved PL spectra were recorded by a gated charge-coupled-device camera with a resolution of $\lesssim 2$ ns. Spatially inhomogeneous excitation was avoided by overlapping the pump and probe excitation spots, each with a diameter of ~ 500 μm, and collecting the PL from the central part of this spot with a diameter of ~ 50 μm.

III. MAGNETIZATION DYNAMICS IN TYPE-II DMS HETEROSTRUCTURES

The DMS heterostructures $Zn_{1-x}Mn_xSe/Be_{1-y}Mn_yTe$ have type-II band alignment with a potential-energy minimum for conduction-band electrons in the $Zn_{1-x}Mn_xSe$ layers and for valence-band holes in the $Be_{1-y}Mn_yTe$ layers. The large difference in band gaps, which are about 2.8 eV for $Zn_{1-x}Mn_xSe$ and 4.5 eV for $Be_{1-y}Mn_yTe$, and huge band offsets of $\gtrsim 2$ and ~ 1 eV for conduction and valence bands, respectively, prevent penetration of the electron and hole wave functions into the neighboring layers. Details of the growth, band structure, and optical properties of these structures can be found in previous publications.[14,15]

We studied three MQW samples with type-II band alignment: sample #1 with parameters $Zn_{0.99}Mn_{0.01}Se/BeTe$ (20/10 nm thicknesses), sample #2 with $Zn_{0.99}Mn_{0.01}Se/Be_{0.93}Mn_{0.07}Te$ (20/10 nm), and sample #3 with $Zn_{0.99}Mn_{0.01}Se/Be_{0.93}Mn_{0.07}Te$ (10/5 nm). Each sample has ten periods of these layer sequences. Sample #1 does not contain Mn in the BeTe layers and serves as reference for sample #2, which only differs by the presence of Mn in the $Be_{0.93}Mn_{0.07}Te$ layers. The main difference between samples #2 and #3 is the thickness of the $Zn_{0.99}Mn_{0.01}Se$ layer of 20 nm and 10 nm, respectively. This results in different distances for spin diffusion from the center of these layers to the interfaces with $Be_{0.93}Mn_{0.07}Te$.

In Figs. 1(a) and 1(b), the band diagrams for the studied type-II structures are shown. The spatially direct (DT) and indirect (IT) optical transitions are indicated by arrows. In the photoluminescence spectra, they appear as emission lines at ~ 2.8 eV and ~ 1.8 eV, respectively, as can be seen in the insets of Fig. 2. In our experiment, the photons from both the pump and probe laser are absorbed by the $Zn_{1-x}Mn_xSe$ layers only. Hence, the indirect emission line is attributed to holes

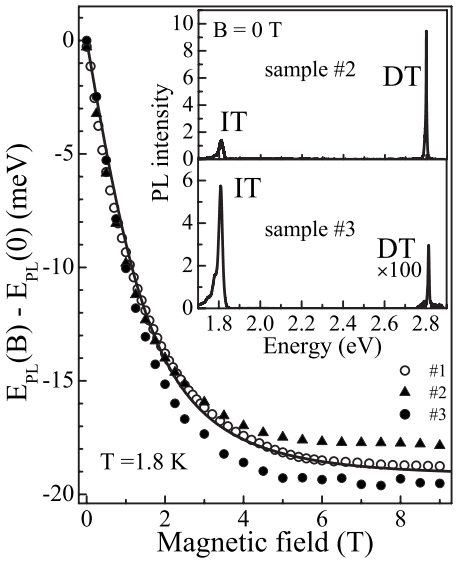

FIG. 2. Giant Zeeman shift of the spatially direct PL line in different $Zn_{1-x}Mn_xSe/Be_{1-y}Mn_yTe$ QWs. Experimental data are shown by symbols, the solid line is a fit for sample #1 with parameters given in the text. In the insets, the photoluminescence spectra of samples #2 and #3 are shown.

scattered from the $Zn_{1-x}Mn_xSe$ into the $Be_{1-y}Mn_yTe$ layers after photogeneration. This hole relaxation process is fast and depends strongly on the width of the $Zn_{1-x}Mn_xSe$ layer.[16,17] As a result, the relative intensities of the direct and indirect emission lines in the samples #2 and #3 (note the multiplication factor for the DT line of sample #3) differ considerably. Since we are interested in the magnetization dynamics of the $Zn_{1-x}Mn_xSe$ layers, we will focus on the giant Zeeman shift of the DT line in the following.

Due to the strong exchange interaction of the free carriers with the localized spins of the Mn^{2+} ions, the exciton transitions in DMS show a giant Zeeman shift in external magnetic fields. This shift equals to one half of the giant Zeeman splitting of the exciton commonly described by the modified Brillouin function, for details see, e.g., Eqs. (1) and (2) in Ref. 6. The experimental data for the giant Zeeman shift in the three studied samples are shown in Fig. 2. The samples show similar shifts saturating at a level of ~18–20 meV, which confirms that the static magnetic properties of the $Zn_{0.99}Mn_{0.01}Se$ layers are not affected by the presence or absence of Mn ions in the adjacent layers. This is expected, as the Mn-carrier exchange interaction has a short-range character and the carrier wave functions are strongly localized in the $Zn_{0.99}Mn_{0.01}Se$ layers.[17,18] The solid line in Fig. 2 is a fit of the experimental data by the modified Brillouin function for sample #1, using the following parameters: $S_{eff}=2.26$, $T_0=1$ K, and $x=0.011$. Similar fits for samples #2 and #3 show that the Mn concentrations in the $Zn_{1-x}Mn_xSe$ layers of all three samples differ by less than 8%. Therefore, their dynamical behaviors can be directly compared with each other.

The dynamics of magnetization relaxation after pump pulse heating are illustrated for the three samples in Figs. 3 and 4. In sample #1, the relaxation time $\tau_{MR} \approx 200$ μs coincides well with the SLR time measured for $Zn_{0.99}Mn_{0.01}Se$

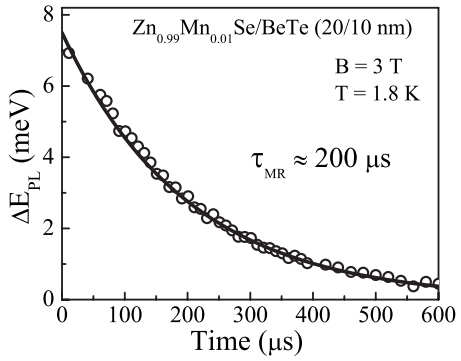

FIG. 3. Temporal evolution of the changes in spectral position of the PL line ΔE_{PL} in the $Zn_{0.99}Mn_{0.01}Se/BeTe$ (20/10 nm) MQW, sample #1.

QWs.[6] Indeed, for this sample no contribution of spin diffusion to the magnetization relaxation is expected, as only the $Zn_{0.99}Mn_{0.01}Se$ layers contain Mn ions.

In comparison with sample #1, a strong reduction in τ_{MR} down to 6 μs is found in sample #2. Obviously, this is due to spin diffusion from the $Zn_{0.99}Mn_{0.01}Se$ to the $Be_{0.93}Mn_{0.07}Te$ layers, where the spin-lattice relaxation time is expected to be short ($\lesssim$200 ns), see Fig. 1(c). Note, that similar results were observed for similar samples in experiments, in which pulses of nonequilibrium phonons were used for heating the Mn spin system.[12]

A further shortening of τ_{MR} down to 1.7 μs in sample #3 (by a factor of about 4 compared to sample #2) originates from a twice smaller distance for spin diffusion between the centers of the $Zn_{0.99}Mn_{0.01}Se$ layers and the interfaces to $Be_{0.93}Mn_{0.07}Te$. We conclude from these experimental data that the spin diffusion in $Zn_{0.99}Mn_{0.01}Se$ can provide spin transfer over distances exceeding 10 nm. We will show in the following Sec. IV that the results of Figs. 3 and 4 are sufficient for evaluating the spin-diffusion coefficient, which makes heteromagnetic structures well suited for quantitative studies of spin diffusion in DMS.

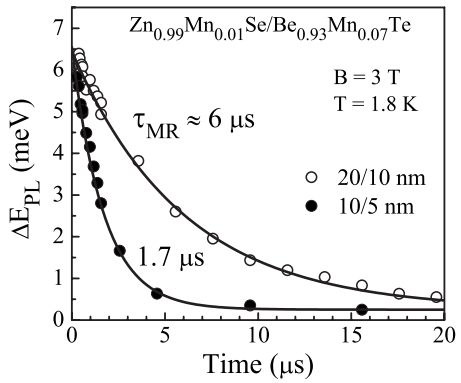

FIG. 4. Temporal evolutions of the changes in spectral position of PL line ΔE_{PL} in two $Zn_{0.99}Mn_{0.01}Se/Be_{0.93}Mn_{0.07}Te$ structures with different layer thicknesses: 20/10 nm (sample #2—open circles) and 10/5 nm (sample #3—closed circles).

IV. NUMERICAL SIMULATIONS OF MAGNETIZATION DYNAMICS

The magnetic relaxation time τ_{MR}, extracted from the dynamical shift of the PL line, can be considered as spin-lattice relaxation time τ_{SLR} only in case of uniformly distributed disordered magnetic ions. As discussed in Sec. III, the spin diffusion in structures with a nonuniform Mn distribution may strongly accelerate the magnetic relaxation. Generally, when the Mn concentration $x(z)$ varies along the growth direction z, the magnetization $M(z)$, and the Mn spin temperature $T_{Mn}(z)$ also depend on z during magnetization relaxation. Hence, the spectral position of the PL line, E_{PL}, is determined by the spatially varying magnetization averaged over the wave functions of the carriers involved in the recombination. In this case, information about the temporal changes in the spatial T_{Mn} profile and, thus, about the local magnetization is important for an adequate description of the experimentally obtained dynamics $\Delta E_{PL}(t)$. We have developed a numerical model allowing direct comparison with experiment on the different samples.

A. Concentration dependence of SLR dynamics

The experimental results for the SLR dynamics of the Mn spin system are summarized in Fig. 1(c), where the SLR time is plotted versus Mn concentration. The open circles are data for $Zn_{1-x}Mn_xSe$-based structures, the data for $Cd_{1-x}Mn_xTe$ are given by the closed symbols.[6] The SLR times cover five orders of magnitude from 10^{-3} down to 10^{-8} s as the Mn concentration varies from 0.004 to 0.11. Such a strong dependence evidences that Mn-Mn interactions play a key role in the SLR dynamics. The results for both materials closely coincide, thus demonstrating that the SLR of the Mn^{2+} ions is rather insensitive to the ion host material.

We turn now to the mechanisms responsible for the strong dependence of the SLR time $\tau_{SLR}(x)$ on the Mn concentration. It is known that an isolated Mn^{2+} ion does not couple to the lattice in a perfect II-VI semiconductor crystal[19] and, therefore, the SLR time should be extremely long. This expectation is based on the following: the electric field of phonons does not act on the magnetic moments of $3d$ electrons and also the magnetic field, induced by temporal variation in the electric field, is relativistically small. In principle, gradients of the electric field may interact with the quadrupole moment of the magnetic ion which, in turn, interacts with the spin. But for Mn^{2+} ions, the d shell is half-filled with electrons so that its quadrupole moment vanishes. In this case, the dominating mechanism of spin-phonon interaction is caused by the phonon modulation of the spin-spin interaction between neighboring Mn ions. The phonons modulate the distance between these ions. Hence, the local exchange field of an ion fluctuates, known as the Waller mechanism,[19] which is obviously strongly dependent on the concentration of magnetic ions. Only the anisotropic exchange interaction is relevant because its operator does not commute with the Zeeman interaction.

The spin-spin interactions between Mn^{2+} ions are provided by three mechanisms: the exchange interaction, the Dzyaloshinsky-Moriya interaction,[20,21] and the magnetic dipole interaction. All of them decrease with increasing distance between Mn ions, where the magnetic dipole interaction is longest ranged. Therefore, despite being relatively weak, it gives the dominant contribution to SLR dynamics in the limit of small Mn concentrations. The exchange and Dzyaloshinsky-Moriya interactions gain importance for higher Mn contents, when the formation of Mn clusters becomes more probable. Both the number of Mn spins in clusters as well as the typical cluster size steadily increase with growing Mn concentration.[22] This is the reason for the strong dependence of SLR time on Mn concentration.[9,23,24] In the frame of a simple model which accounts for spin diffusion from Mn ions to Mn clusters, where the spin undergoes relaxation, it can be shown that the SLR rate $1/\tau_{SLR}$ has a strong dependence on the Mn content with a power law between x^3 and x^4 (Ref. 11). This is in good qualitative agreement with the experimental data in Fig. 1(c).

According to Fig. 1(c), one can conclude that for fixed external conditions the Mn concentration x mainly determines the SLR dynamics. This establishes a relationship between static and dynamic magnetization, e.g., between the giant Zeeman splitting and the SLR time, both depending on Mn content. This restrictive interdependence can be relaxed or even canceled by growth of heterostructures with modulated Mn content and/or modulation doping by donors or acceptors providing free carriers. In Sec. V, examples of such structures are discussed, where the magnetization dynamics has been considerably accelerated without changing the static magnetization.

B. Model

The magnetization $M(B,T_{Mn})$ in DMS is a function of magnetic field and the Mn spin temperature,[3]

$$M(B,T_{Mn}) = g\mu_B x N_0 S_{eff}(x) B_{5/2}\left\{\frac{5g\mu_B B}{2k_B[T_{Mn}+T_0(x)]}\right\}. \quad (1)$$

Here N_0 is the inverse unit-cell volume, $B_{5/2}$ is the modified Brillouin function, $g=2.01$ is the g factor of Mn^{2+} ions, k_B is the Boltzmann constant and μ_B is the Bohr magneton. $S_{eff}(x)$ is the effective spin and $T_0(x)$ is the effective temperature. These two parameters account for the antiferromagnetic Mn-Mn interactions contributing to the overall magnetization.[25,26] In equilibrium, the Mn spin temperature is equal to the temperature of the phonon bath: $T_{Mn}=T_L$.

The model should take into account the processes of spin diffusion and spin-lattice relaxation in the Mn spin system. It should also describe the relaxation the magnetization changes $|\Delta M(\Delta T_{Mn})|=|M(T_{Mn})-M(T_L)|$ induced by an external perturbation in a magnetic field. In this nonequilibrium situation, the spin temperature difference is given by $\Delta T_{Mn}=T_{Mn}-T_L$. In DMS with a homogeneous Mn concentration x, which does not vary spatially, the magnetization dynamics in the one-dimensional case can be described by

$$\frac{\partial}{\partial t}|\Delta M| = K_{diff}(x)\frac{\partial^2}{\partial z^2}|\Delta M| - \frac{|\Delta M|}{\tau_{SLR}(x)}. \quad (2)$$

Here $K_{diff}(x)$ is the spin-diffusion coefficient. For dipole-dipole interaction between the Mn^{2+} spins, the dependence of

K_{diff} on the Mn concentration x can be expressed as

$$K_{\mathrm{diff}}(x) = K_0 x^{4/3}, \tag{3}$$

where K_0 is the spin-diffusion constant, see Eq. (3.25) in Ref. 27.

Using Eq. (1), Eq. (2) can be written in terms of ΔT_{Mn},

$$\frac{\partial}{\partial t}\Delta T_{\mathrm{Mn}} = K_{\mathrm{diff}}(x)\frac{\partial^2}{\partial z^2}\Delta T_{\mathrm{Mn}} - \frac{|\Delta M|}{\tau_{\mathrm{SLR}}(x)}\left[\frac{dM(T_{\mathrm{Mn}})}{dT_{\mathrm{Mn}}}\right]^{-1}. \tag{4}$$

For small deviations from equilibrium and/or if M is a linear function of T_{Mn}, the last term is equal to $\Delta T_{\mathrm{Mn}}/\tau_{\mathrm{SLR}}$. It should be noted that for the ranges of B and T_{Mn}, relevant for the present publication, the relation between the magnetization changes ΔM and ΔT_{Mn} is close to linear. Therefore, we suggest that the relaxation of ΔT_{Mn} is simply determined by τ_{SLR}.

Equation (4) can be generalized to the case of nonuniform Mn distributions $x(z)$ along the growth direction z of the heterostructure,

$$\frac{\partial}{\partial t}\Delta T_{\mathrm{Mn}} = \frac{\partial}{\partial z}\left[K_{\mathrm{diff}}(z)\frac{\partial}{\partial z}\Delta T_{\mathrm{Mn}}\right] - \frac{\Delta T_{\mathrm{Mn}}}{\tau_{\mathrm{SLR}}(z)}. \tag{5}$$

In the model we suggest that the spin-diffusion coefficient $K_{\mathrm{diff}}(z)$ is determined by the local Mn concentration $x(z)$ according to Eq. (3). An additional assumption is that the SLR time is determined by the local Mn concentration $x(z)$. For the dependence $\tau_{\mathrm{SLR}}(x)$, we used the interpolation function shown in Fig. 1(c) by the solid line.

In order to compare the experiment and theory, the calculations were performed in two steps. First, we solved numerically the one-dimensional partial differential Eq. (5), which describes the dynamics of the spatial T_{Mn} distribution in samples with nonuniform concentration of magnetic ions, as an initial boundary-value problem. We chose an uniform-in-space distribution of T_{Mn} as initial condition. The solution gives us information about T_{Mn} at different points in space and different moments in time. An example of such calculation, which will be discussed in detail below, is shown in Fig. 6.

The second step comprises the numerical solution of the Schrödinger equations for electrons and holes. The potential profiles for carriers in DMS depend on the external magnetic field strength and Mn spin temperature due to the giant Zeeman effect. The corresponding energy shifts of conduction and valence bands are described by

$$\Delta E_{e(h)}(B, T_{\mathrm{Mn}}) = \frac{\alpha_{e(h)}}{\mu_{\mathrm{B}} g} M(B, T_{\mathrm{Mn}}), \tag{6}$$

where $N_0\alpha_e$ and $N_0\alpha_h$ are the exchange constants for conduction and valence band. In $Zn_{1-x}Mn_xSe$ they are equal to 0.26 and −1.31 eV, and in $Cd_{1-x}Mn_xTe$ they are equal to 0.22 and −0.88 eV, respectively.[4] The Mn spin temperature distribution $T_{\mathrm{Mn}}(z,t)$, obtained by numerical solution of Eq. (5), allows us to determine the exact potential profiles for electrons and holes in external magnetic field at different times after pulsed heating of the Mn spin system. For every moment of time, we solved numerically the Schrödinger equations to obtain the electron and hole energies. This, in turn, allows us to calculate the changes in the spectral position of the PL line and to compare it with the experimental data for $\Delta E_{\mathrm{PL}}(t)$.

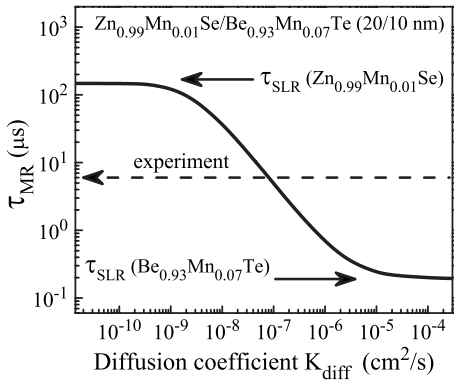

FIG. 5. Calculated dependence of magnetic relaxation time τ_{MR} on diffusion coefficient K_{diff} in the $Zn_{0.99}Mn_{0.01}Se$ layer of the $Zn_{0.99}Mn_{0.01}Se/Be_{0.93}Mn_{0.07}Te$ (20/10 nm) QW. In the limiting cases of small and large K_{diff} the magnetic relaxation time is determined by τ_{SLR} in $Zn_{0.99}Mn_{0.01}Se$ and $Be_{0.93}Mn_{0.07}Te$, respectively. Dashed line shows experimental value of $\tau_{\mathrm{MR}} \approx 6$ μs.

C. Numerical results for type-II DMS heterostructures

In this section, we present the results of numerical simulations of magnetic relaxation dynamics in the type-II $Zn_{0.99}Mn_{0.01}Se/Be_{0.93}Mn_{0.07}Te$ (20/10 nm) MQW (sample #2). The experimental data for this structure are shown in Fig. 4. The Mn profile $x(z)$ in this structure, which we used to solve Eq. (5), is a steplike function with values of 0.01 and 0.07 in the adjacent layers. The SLR times τ_{SLR} in $Zn_{0.99}Mn_{0.01}Se$(~200 μs) and $Be_{0.93}Mn_{0.07}Te$(≲200 ns) differ by more than 3 orders of magnitude. In that case the $Be_{0.93}Mn_{0.07}Te$ layers serve as an efficient SLR channel for spin excitations arriving there by diffusion from the $Zn_{0.99}Mn_{0.01}Se$ layers. The results of numerical simulations are nearly independent of spin diffusion inside the $Be_{0.93}Mn_{0.07}Te$ layers and are predominantly controlled by K_{diff} in the $Zn_{0.99}Mn_{0.01}Se$ layers. Therefore, this type of heteromagnetic heterostructure offers a reliable tool for evaluating K_{diff}.

In Fig. 5, the calculated dependence of τ_{MR} on K_{diff} is shown by the thick solid line. The magnetic relaxation times for this dependence were used as characteristic times for the calculated $\Delta E_{\mathrm{PL}}(t)$ dynamics. These times were determined at the points where the normalized $\Delta E_{\mathrm{PL}}(t)$ is reduced to $1/e = 0.37$ of its original value. Thus, the results in Fig. 5 can be directly compared with experiment. As expected, the extreme values of $K_{\mathrm{diff}} \to 0$ and $\to \infty$ reflect the identity $\tau_{\mathrm{MR}} = \tau_{\mathrm{SLR}}$ in the $Zn_{0.99}Mn_{0.01}Se$ and $Be_{0.93}Mn_{0.07}Te$ layers, respectively. The dashed arrow in Fig. 5 indicates the experimental value for $\tau_{\mathrm{MR}} \approx 6$ μs, measured for sample #2 (see Fig. 4). From its crossing point with the solid line, we evaluate the spin-diffusion coefficient in $Zn_{0.99}Mn_{0.01}Se$ with rather high accuracy to $K_{\mathrm{diff}} \approx (7 \pm 1.5) \times 10^{-8}$ cm^2/s. Consequently, according to Eq. (3) the diffusion constant is $K_0 \approx 3.5 \times 10^{-5}$ cm^2/s. To the best of our knowledge, experimental evaluation of the spin-diffusion parameters in DMS had not been achieved so far.

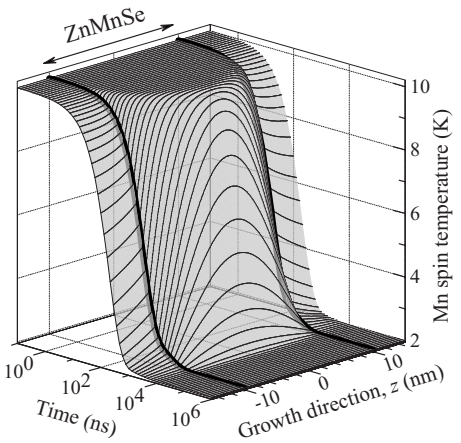

FIG. 6. Calculated temporal and spatial distribution of Mn spin temperature in the $Zn_{0.99}Mn_{0.01}Se/Be_{0.93}Mn_{0.07}Te$ QW (20/10 nm). Initially, $T_{Mn}=10$ K is uniform in space, the final temperature is $T_{Mn}=T_L=2$ K, $K_{diff}=7\times10^{-8}$ cm^2/s in the $Zn_{0.99}Mn_{0.01}Se$ layer. Thick solid lines show temperatures close to the interfaces.

Let us take now a closer look at the calculated spatial and temporal profiles of T_{Mn} in the heteromagnetic structure #2 (see Fig. 6). The initial condition for this numerical problem was that the Mn spin system of the whole sample is heated homogeneously up to $T_{Mn}=10$ K, which can be seen by the flat temperature level at short time delays. In our experiments such heating was provided by interaction of Mn ions with photogenerated carriers. The subsequent magnetic relaxation in the Mn spin system is provided by SLR and spin diffusion. The latter is responsible for the spatially inhomogeneous cooling of the Mn spin system in the $Zn_{0.99}Mn_{0.01}Se$ layer, clearly visible in Fig. 6. At time delays exceeding 20 μs all Mn spins reach the equilibrium temperature of the phonon bath, which was chosen to be $T_L=2$ K.

For more detailed insight the spatial profiles of $T_{Mn}(z)$ at different time delays are shown in Fig. 7(a). In fact, these profiles are cross sections of Fig. 6 at fixed time delays ranging from 0.1 to 100 μs. In order to demonstrate the importance of spin diffusion for magnetic relaxation in this structure we present in Fig. 7(b) the calculated results for absence of spin diffusion, i.e., for $K_{diff}=0$. It is equivalent with independent relaxation of T_{Mn} in the adjacent layers with the corresponding SLR times. The temperature profiles in each layer are flat. Also, the relaxation of T_{Mn} for Mn ions located, e.g., in the vicinity of the center of the $Zn_{0.99}Mn_{0.01}Se$ layer is considerably slower than for a finite diffusion coefficient, as shown in Fig. 7(a).

Figure 8 demonstrates the dynamics of T_{Mn} in the center of the $Zn_{0.99}Mn_{0.01}Se$ layer, which strongly depends on K_{diff} in this layer. For $K_{diff}=0$ spin diffusion is absent so that the relaxation process is solely controlled by the SLR time in the $Zn_{0.99}Mn_{0.01}Se$ layer, which is approximately 200 μs. In contrast, if the value of $K_{diff}\rightarrow\infty$, and, thus, the spin-diffusion time does not restrict the magnetic relaxation time, the Mn spin temperature drops very fast to the bath value of $T_{Mn}=T_L=2$ K, and is controlled only by the SLR time ($\lesssim$200 ns) in the $Be_{0.93}Mn_{0.07}Te$ layers. The calculated dynamics of T_{Mn} with $K_{diff}=7\times10^{-8}$ cm^2/s, which corresponds to the experimental situation for sample #2, is shown by the dashed line in Fig. 8.

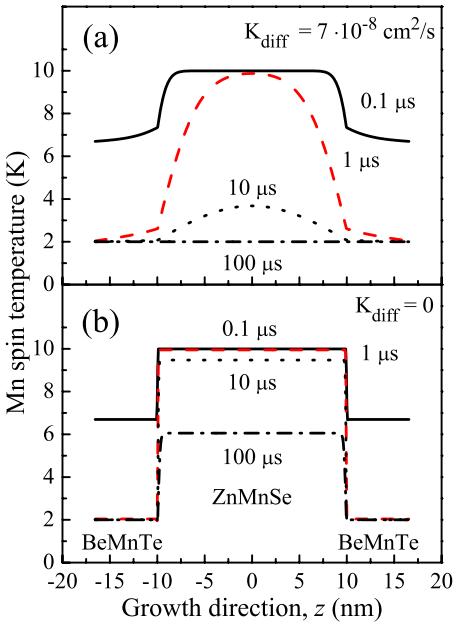

FIG. 7. (Color online) Calculated spatial distribution of Mn spin temperature in the $Zn_{0.99}Mn_{0.01}Se/Be_{0.93}Mn_{0.07}Te$ QW (20/10 nm) at different time delays after pump pulse. Panels (a) and (b) correspond to different values of K_{diff} in the $Zn_{0.99}Mn_{0.01}Se$ layer. Initial and final temperatures are 10 K and 2 K, respectively.

V. MAGNETIZATION DYNAMICS IN CdTe/CdMnTe STRUCTURES TAILORED BY DIGITAL GROWTH

The digital growth technique has achieved about atomic precision by using molecular-beam epitaxy. It has been implemented for GaAs/AlAs heterostructures, for which during growth wide-band-gap AlAs layers with a certain thickness (frequently submonolayer) are introduced into narrow-band-gap GaAs layers.[28] This technique allows a high variability of the shape of the confining potential in quantum well structures. Also, by growing periodic structures with layer thicknesses of the order of a single monolayer (ML) a digital alloy (DA) can be fabricated, whose properties can significantly differ from the properties of common disordered alloys, e.g., $Al_xGa_{1-x}As$.

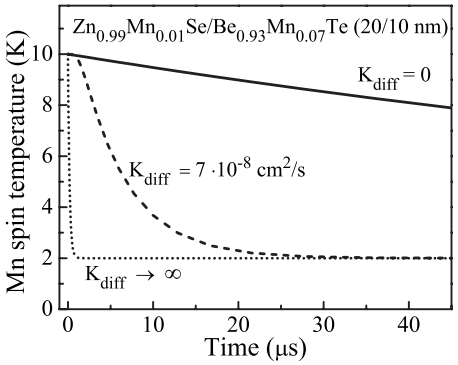

FIG. 8. Temporal evolution of Mn spin temperature in the center of the $Zn_{0.99}Mn_{0.01}Se$ layer calculated for different values of diffusion coefficient K_{diff}. Initial and final temperatures are 10 and 2 K, respectively.

Digital growth was successfully established also for DMS heterostructures.[13,29] For the $CdTe/Cd_{1-x}Mn_xTe$ material system, digital alloys and parabolic quantum wells were grown.[10,30] In these structures, the band-gap profile is controlled by implementation of Mn ions, and, thereby, the magnetic properties become also modulated. It was shown experimentally that the partial smoothing of the digitally grown Mn profile considerably reduces the possible modifications of the static magnetic properties due to Mn intermixing with neighboring CdTe layers.[31,32] Typically, the latter are measured optically via the giant Zeeman splitting of excitons. However, the magnetization dynamics can be changed drastically.[10] Such a difference in static and dynamical magnetization properties can be explained by different underlying mechanisms. The static magnetization is mainly contributed by the paramagnetic Mn spins while the magnetization dynamics critically depends on the concentration of Mn clusters serving as spin-relaxation centers.

In this section, we analyze the Mn spin dynamics in two types of $CdTe/Cd_{1-x}Mn_xTe$ heterostructures: digital alloys and parabolic QWs. We demonstrate that spin diffusion in the Mn spin system plays a key role in its dynamics, which can be confirmed by numerical simulations.

A. CdTe/CdMnTe digital alloys

Let us analyze the experimental results for three samples with $CdTe/Cd_{1-x}Mn_xTe$ digital alloys presented in Ref. 10. In these samples, 23-nm-thick $Cd_{0.95}Mn_{0.05}Te/CdTe$ DA layers (corresponding to about 70 monolayers) are placed between nonmagnetic $Cd_{0.8}Mg_{0.2}Te$ barriers. According to the thicknesses of magnetic and nonmagnetic layers (given in monolayers), the structures are labeled in the following way: the first sample 1×3 DA consists of 18 periods of 1 ML/3 ML, the second sample 2×6 DA has 9 periods of 2 ML/6 ML, and the third sample 3×9 DA has 6 periods of 3 ML/9 ML. This choice of layer thicknesses provides the same average Mn concentration $x_{DA}\approx0.013$ in the three samples.

The experimental data for excitonic giant Zeeman shifts and magnetic relaxation dynamics, measured in Ref. 10, are shown by symbols in Figs. 9(a) and 9(b), respectively. The Zeeman shifts of the three samples follow closely each other with rather small differences in the saturation levels at high magnetic fields. This reflects that the static magnetization is mainly controlled by the average Mn concentration in the DAs.

In contrast, the magnetic relaxation dynamics in the DAs strongly depends on the details of the real, smoothed Mn profiles. As one can see in Fig. 9(b), the magnetic relaxation times shorten from 9.5 μs in 1×3 DA to 2.5 μs in 3×9 DA. They considerably deviate from the relaxation time of 27 μs, measured in the disordered $Cd_{0.985}Mn_{0.015}Te$ reference alloy.[10]

We simulated numerically the magnetic relaxation dynamics in these DAs. For that purpose, we smoothed the nominal technological profile by accounting for Mn intermixing, i.e., we took the convolution of this profile with an exponential broadening function,[31]

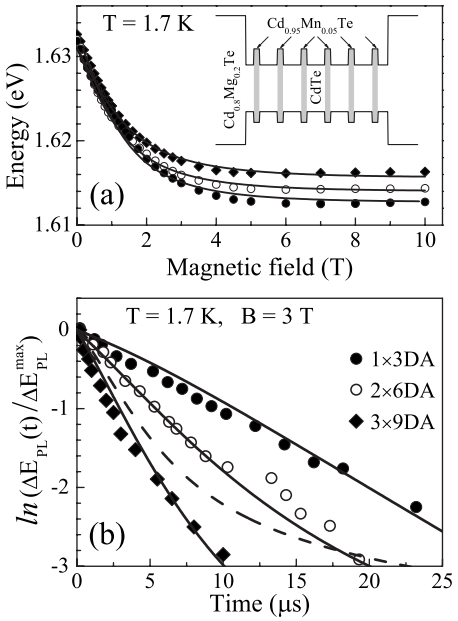

FIG. 9. (a) Giant Zeeman shift vs magnetic field and (b) dynamical shift of the exciton PL lines $\Delta E_{PL}(t)$ during magnetic relaxation in three digital alloy samples. The sample design is shown schematically in the inset. Experimental data in both panels, shown by symbols, were taken from Ref. 10. Solid lines are results of numerical calculations. For the modeling values of the diffusion coefficient $K_{diff}=3.5\times10^{-5}x^{4/3}$ [cm^2/s] and Mn intermixing length $l_0=0.3$ nm were used. The dashed line in panel (b) represents calculated results for the 2×6 DA sample, neglecting spin diffusion ($K_{diff}=0$).

$$g(z)=\begin{cases}\exp(z/l_0-1), & z<l_0\\ 0, & z\geq l_0.\end{cases} \tag{7}$$

Then we solved Eq. (5) by using the diffusion coefficient Eq. (3) with $K_0=3.5\times10^{-5}$ cm^2/s, as estimated in Sec. IV. We realized that the Mn intermixing length l_0 strongly controls the relative ratio of the τ_{MR} in the three different DA samples, which allows a high-precision evaluation of $l_0\approx0.3$ nm. It is important to stress here, that even though the magnetic relaxation in the DAs does not follow a single exponential law, it can still be rather well fitted by such a form, compare solid lines and symbols in Fig. 9(b). It is also interesting that, despite the small layer thicknesses in the DAs, consideration of spin diffusion in the Mn spin system was important. The dashed line in Fig. 9(b) shows the calculated result for the 2×6 DA sample in absence of spin diffusion ($K_{diff}=0$). It considerably deviates from the experimental data.

Using the Mn intermixing length $l_0=0.3$ nm, evaluated from the best fit of magnetic relaxation dynamics, we calculated the giant Zeeman shift and obtained good accordance with experimental data, as the solid lines and symbols in Fig. 9(a) show. This makes us confident that the used numerical approach properly accounts for the main factors controlling the static and dynamic magnetization in the studied DAs.

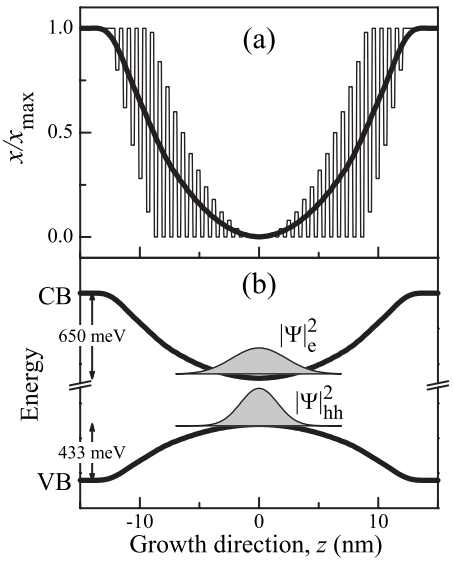

FIG. 10. (a) The thin line represents the designed profile of the Mn concentration in 25.4-nm-thick $CdTe/Cd_{1-x}Mn_xTe$ parabolic QW. The effective averaged Mn concentration is given by the thick line (see text). (b) Effective conduction- and valence-band profiles for parabolic QW with $x_{max}=0.68$. Gray areas show squared moduli of the ground-state wave functions of electrons and heavy holes.

B. CdTe/CdMnTe parabolic QWs

The digital growth technology enables fabrication of structures with continuously varying the Mn concentration and potential profile along the growth direction. An interesting example of these possibilities is a parabolic $CdTe/Cd_{1-x}Mn_xTe$ QW, where the confinement potential for the QW carriers can be described by a parabola along growth direction. Details about growth and magneto-optical properties of such QWs can be found in Refs. 30, 33, and 34.

We measured the magnetic relaxation dynamics for two parabolic QWs with different maximal Mn contents x_{max} of 0.13 and 0.68. Both QWs have a thickness of 25.4 nm, which corresponds to 82 monolayers (one monolayer of CdTe has 0.324 nm thickness). The Mn shutter was continuously opened for growth of the barriers and periodically shut and opened during growth of the parabolic QW. The QW growth was divided into 41 steps. In each step the Mn cell was opened for the time needed to obtain a certain Mn concentration, more details can be found in Ref. 30. The targeted Mn profile averaged over each monolayer is shown by the thin solid line in Fig. 10(a). After smoothing one obtains a parabolic profile represented by the thick line. In real structures, the Mn intermixing is not sufficient to reach the continuous Mn distribution shown by the solid line, only the sharp boundaries in the nominal Mn profile are smeared.

The carrier wave functions, for both electrons in the conduction band and heavy holes in the valence band, penetrate through the digital layers. As a result, their quantum-well confinement potentials can be well approximated by the parabolas shown in Fig. 10(b) by thick lines. The squared moduli of the ground-state wave functions, calculated in realistic potentials for $x_{max}=0.68$ and Mn intermixing length $l_0=0.3$ nm, are shown by gray areas in Fig. 10(b). The electrons and holes are localized close to the center of the parabolic QW. Details about carrier energy levels and exciton giant Zeeman splitting in $CdTe/Cd_{1-x}Mn_xTe$ parabolic QWs are given in Refs. 33 and 34.

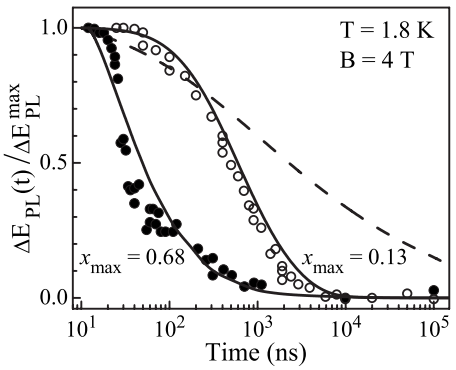

FIG. 11. Magnetic relaxation dynamics in 25.4-nm-thick $CdTe/Cd_{1-x}Mn_xTe$ parabolic quantum wells with different x_{max}. Solid lines are calculated results with $K_{diff}=3.5\times10^{-5}x^{4/3}$ [cm^2/s] and $l_0=0.3$ nm. Dashed line shows calculated results for the sample with $x_{max}=0.68$ without taking into account spin diffusion ($K_{diff}=0$).

Experimental results on the magnetic relaxation dynamics, measured through the dynamical shift of the exciton PL line ΔE_{PL}, are shown by the symbols in Fig. 11. The characteristic times τ_{MR} for the samples with $x_{max}=0.13$ and 0.68 differ considerably, being ~1 μs and ~100 ns, respectively. This difference can be explained by Mn clustering, controlling τ_{SLR}, and by Mn spin diffusion.

One should expect that in these relatively thick structures with gradual variation in the magnetic properties from the QW center to its edges spin diffusion in the Mn spin system plays an important role for magnetic relaxation. In fact, its significance for the sample with $x_{max}=0.68$ is pointed out by comparing the calculations with (solid line in Fig. 11) and without (dashed line) spin diffusion. The very long relaxation tail without spin diffusion (note the logarithmic time scale) is due to long SLR times in the region of low Mn concentration nearby the QW center. This region is essential for the dynamics of exciton giant Zeeman shift, as the electron and hole wave functions are primarily concentrated there, see Fig. 10(b).

Further, the numerical results presented in Fig. 11 coincide with the experimental data for the parabolic QWs with very different $x_{max}=0.68$ and 0.13 without changing the parameters ($K_{diff}=3.5\times10^{-5}x^{4/3}$ [cm^2/s], $l_0=0.3$ nm). This fact is very promising for describing the magnetic relaxation dynamics in such complicated structures in the frame of a relatively simple model without fitting parameters. This also makes us confident that the suggested functional dependence Eq. (3) of the diffusion coefficient on Mn content is well suited for modeling the magnetization dynamics.

VI. DISCUSSION AND CONCLUSIONS

Note, that even in bulk disordered DMS samples with a homogeneous distribution of Mn ions spin diffusion can have

a significant role for the magnetic relaxation dynamics. This can be attributed to at least two reasons: (i) spatially inhomogeneous heating of the Mn spin system, e.g., by a tightly focused laser beam. Based on typical parameters for the studied materials, we estimate that the length scale of such an inhomogeneity should be smaller than 1 μm. (ii) Intrinsic instabilities in the highly excited Mn spin system, which may lead to formation of domains with "hot" and "cold" spin temperatures, whose size and dynamics are governed by spin diffusion.[35–37] These conclusions are similarly true for heterostructures containing layers with only one Mn concentration, e.g., DMS quantum wells confined by nonmagnetic barriers.

It is known that the SLR dynamics of Mn ions is strongly accelerated by an increase in lattice temperature[9,38] and also becomes faster in stronger external magnetic fields.[38,39] Clearly, such effects modify the magnetic relaxation dynamics in heteromagnetic heterostructures, which strongly depends on τ_{SLR}.

In addition to that spin diffusion can be a dominating factor for the magnetic relaxation dynamics in epitaxially grown DMS quantum dots. Such quantum dots are typically grown on top of a (about one monolayer thick) wetting layer, whose effective Mn concentration (due to the small thickness, see discussion in the section on digital alloys) is considerably smaller than in the quantum dots. Experimental data available for such dots show a strongly nonexponential magnetic relaxation, which has been tentatively explained by spin diffusion between the Mn spin systems of the quantum dots and the wetting layer.[8,40] DMS quantum dots have a faster SLR compared to the wetting layer but they are characterized by a very limited capacity of the spin reservoir. In this case, spin diffusion would control the heating of the Mn spin system in contrast to the cooling scenarios considered in the present paper.

In conclusion, we performed detailed experimental and theoretical investigations of the magnetic relaxation dynamics in different types of DMS quantum wells. We showed that spin diffusion in the Mn spin system plays an important role in these dynamics, which is especially evident for structures with nonuniform Mn distribution. The diffusion coefficient $K_{diff}=7\times10^{-8}$ cm^2/s was measured for $Zn_{0.99}Mn_{0.01}Se$. The results for parabolic QWs suggest that the functional dependence of the diffusion coefficient on Mn content, $K_{diff}\approx3.5\times10^{-5}x^{4/3}$ $[cm^2/s]$ as obtained from the theoretical approach in Ref. 27, is well suited for modeling in a wide range of Mn concentrations.

ACKNOWLEDGMENTS

We greatly acknowledge the encouraging discussions with R. A. Suris and D. Dunker for the help with experiment. The work has been supported by the Deutsche Forschungsgemeinschaft, the EU Seventh Framework Programme (Grant No. 237252, Spin-optronics) and by the Russian Foundation of Basic Research (Grants No. 08-02-01302 and No. 10-02-00549).

*Corresponding author; maksimov@issp.ac.ru

[1] *Semiconductor Spintronics and Quantum Computation*, edited by D. D. Awschalom, D. Loss, and N. Samarth (Springer-Verlag, Berlin, 2002).

[2] *Spin Physics in Semiconductors*, edited by M. I. Dyakonov (Springer-Verlag, Berlin, 2008).

[3] *Diluted Magnetic Semiconductors*, Semiconductors and Semimetals Vol. 25, edited by J. K. Furdyna and J. Kossut (Academic, London, 1988).

[4] T. Dietl, in *Handbook of Semiconductors*, edited by S. Mahajan (North-Holland, Amsterdam, 1994), Vol. 3b, p. 1252.

[5] B. König, I. A. Merkulov, D. R. Yakovlev, W. Ossau, S. M. Ryabchenko, M. Kutrowski, T. Wojtowicz, G. Karczewski, and J. Kossut, Phys. Rev. B **61**, 16870 (2000).

[6] M. K. Kneip, D. R. Yakovlev, M. Bayer, A. A. Maksimov, I. I. Tartakovskii, D. Keller, W. Ossau, L. W. Molenkamp, and A. Waag, Phys. Rev. B **73**, 045305 (2006).

[7] M. K. Kneip, D. R. Yakovlev, M. Bayer, A. A. Maksimov, I. I. Tartakovskii, D. Keller, W. Ossau, L. W. Molenkamp, and A. Waag, Phys. Rev. B **73**, 035306 (2006).

[8] A. V. Akimov, A. V. Scherbakov, and D. R. Yakovlev, in *Handbook of Semiconductor Nanostructures and Nanodevices*, edited by A. A. Balandin and K. L. Wang (American Scientific Publishers, Los Angeles, 2006), pp. 45–93, Chap. 2.

[9] D. Scalbert, Phys. Status Solidi B **193**, 189 (1996).

[10] M. K. Kneip, D. R. Yakovlev, M. Bayer, G. Karczewski, T. Wojtowicz, and J. Kossut, Appl. Phys. Lett. **88**, 152105 (2006).

[11] R. A. Suris (private communication).

[12] A. V. Scherbakov, A. V. Akimov, D. R. Yakovlev, W. Ossau, L. Hansen, A. Waag, and L. W. Molenkamp, Appl. Phys. Lett. **86**, 162104 (2005).

[13] T. Wojtowicz, G. Karczewski, A. Zakrzewski, M. Kutrowski, E. Janik, E. Dynowska, K. Kopalko, S. Kret, J. Kossut, and J. Y. Laval, Acta Phys. Pol. A **87**, 165 (1995).

[14] D. R. Yakovlev, C. Sas, B. König, L. Hansen, W. Ossau, G. Landwehr, L. W. Molenkamp, and A. Waag, Appl. Phys. Lett. **78**, 1870 (2001).

[15] D. R. Yakovlev, A. V. Platonov, E. L. Ivchenko, V. P. Kochereshko, C. Sas, W. Ossau, L. Hansen, A. Waag, G. Landwehr, and L. W. Molenkamp, Phys. Rev. Lett. **88**, 257401 (2002).

[16] A. A. Maksimov, I. I. Tartakovskii, D. R. Yakovlev, M. Bayer, and A. Waag, JETP Lett. **83**, 141 (2006).

[17] A. A. Maksimov, S. V. Zaitsev, E. V. Filatov, A. V. Larionov, I. I. Tartakovskii, D. R. Yakovlev, and A. Waag, JETP Lett. **88**, 511 (2008).

[18] A. A. Maksimov, S. V. Zaitsev, I. I. Tartakovskii, V. D. Kulakovskii, N. A. Gippius, D. R. Yakovlev, W. Ossau, G. Reuscher, A. Waag, and G. Landwehr, Phys. Status Solidi B **221**, 523 (2000).

[19] A. Abragam and B. Bleaney, *Electron Paramagnetic Resonance of Transition Ions* (Clarendon Press, Oxford, 1970).

[20] I. Dzyaloshinsky, J. Phys. Chem. Solids **4**, 241 (1958).
[21] T. Moriya, Phys. Rev. **120**, 91 (1960).
[22] B. E. Larson, K. C. Hass, and R. L. Aggarwal, Phys. Rev. B **33**, 1789 (1986).
[23] W. Farah, D. Scalbert, and M. Nawrocki, Phys. Rev. B **53**, R10461 (1996).
[24] X. Wang, M. Dahl, D. Heiman, P. A. Wolff, and P. Becla, Phys. Rev. B **46**, 11216 (1992).
[25] D. Keller, D. R. Yakovlev, B. König, W. Ossau, Th. Gruber, A. Waag, L. W. Molenkamp, and A. V. Scherbakov, Phys. Rev. B **65**, 035313 (2001).
[26] J. A. Gaj, R. Planel, and G. Fishman, Solid State Commun. **29**, 435 (1979).
[27] A. I. Burshteĭn, Sov. Phys. Usp. **27**, 579 (1984).
[28] A. C. Gossard, M. Sundaram, and P. F. Hopkins, in *Epitaxial Microstructures*, Semiconductors and Semimetals, edited by A. C. Gossard (Academic Press, Boston, 1994), p. 153.
[29] S. A. Crooker, D. A. Tulchinsky, J. Levy, D. D. Awschalom, R. Garcia, and N. Samarth, Phys. Rev. Lett. **75**, 505 (1995).
[30] T. Wojtowicz, M. Kutrowski, M. Surma, K. Kopalko, G. Karczewski, J. Kossut, M. Godlewski, P. Kossacki, and N. T. Knoi, Appl. Phys. Lett. **68**, 3326 (1996).
[31] J. A. Gaj, W. Grieshaber, C. Bodin-Deshayes, J. Cibert, G. Feuillet, Y. Merle d'Aubigne, and A. Wasiela, Phys. Rev. B **50**, 5512 (1994).
[32] W. Grieshaber, A. Haury, J. Cibert, Y. Merle d'Aubigne, A. Wasiela, and J. A. Gaj, Phys. Rev. B **53**, 4891 (1996).
[33] W. Ossau, R. Fiederling, B. König, T. Wojtowicz, M. Kutrowski, G. Karczewski, and J. Kossut, Physica E **2**, 209 (1998).
[34] T. Wojtowicz, G. Karczewski, and J. Kossut, Thin Solid Films **306**, 271 (1997).
[35] M. G. Tyazhlov, A. I. Filin, A. V. Larionov, V. D. Kulakovskii, D. R. Yakovlev, A. Waag, and G. Landwehr, Sov. Phys. JETP **85**, 784 (1997).
[36] M. G. Tyazhlov, V. D. Kulakovskii, A. I. Filin, D. R. Yakovlev, A. Waag, and G. Landwehr, Phys. Rev. B **59**, 2050 (1999).
[37] M. Vladimirova, D. Scalbert, and C. Misbah, Phys. Rev. B **71**, 233203 (2005).
[38] A. V. Scherbakov, A. V. Akimov, D. R. Yakovlev, W. Ossau, G. Landwehr, T. Wojtowicz, G. Karczewski, and J. Kossut, Phys. Rev. B **62**, R10641 (2000).
[39] T. Strutz, A. M. Witowski, and P. Wyder, Phys. Rev. Lett. **68**, 3912 (1992).
[40] A. V. Scherbakov, A. V. Akimov, D. R. Yakovlev, W. Ossau, L. W. Molenkamp, Y. Terai, S. Kuroda, K. Takita, I. Souma, and Y. Oka, Phys. Status Solidi B **241**, 361 (2004).